Electronic Supplementary Material (ESI) for Materials Advances.
This journal is © The Royal Society of Chemistry 2024

Cold H_2-Ar plasma interaction with nickel α-hydroxide as a versatile nanofabrication tool of Ni@C_{gr} nanoparticles

Marie-Charlotte Dragassi[1,2], Sonia Haj-Khlifa[1,2], Nicolas Menguy[3], Michael Redolfi[2*], Souad Ammar[1*]

[1] Université Paris Cité, CNRS UMR-7086, ITODYS, 15 Rue Jean-Antoine de Baïf, FR-75251 Paris, France.
[2] Université Sorbonne Paris Nord, CNRS UPR-3407, LSPM, 99 avenue Jean-Baptiste Clément, FR-93430 Villetaneuse, France.
[3] Sorbonne Université, CNRS UMR-7590, ICMPC, 2-4 Place Jussieu, FR-75005 Paris, France.

Supporting

Nickel layered hydroxyacetate powder characterization

The X-ray diffraction (XRD) pattern of the produced green powder has a typical feature of a lamellar brucite-type compound (Figure S1a) with sharp reflections in the range of small Bragg angles, the smallest angle corresponding to the 001 plans, allowing us determining the *c* cell parameter value, which corresponds to the stacking direction (11.05 ± 0.01 Å). The pattern had also a typical feature of incompletely ordered brucite structure, since broad and asymmetric reflections in the range of high angles are observed. The brucite-like sheets are parallel and equidistant along the c direction but twisted against each other. The asymmetric peaks are indexed as the hk0 reflections, allowing us to determine the basal plane distances, *a* and *b* (3.13 ± 0.01 Å). Transmission electron microscopy (TEM) observations confirmed these structural features, since the sample appears as non-well defined aggregates of thin crumpled sheets (Figure S1b).

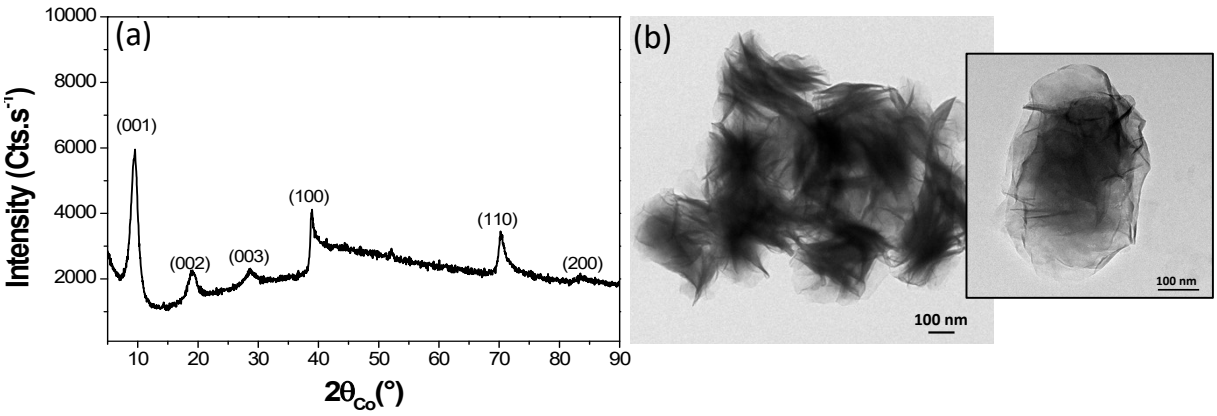

Figure S1. a) XRD pattern of the polyol-made nickel hydroxide powder, fully indexed within the brucite-type structure. b) TEM image of the produced powder with a zoom on one representative particle.

Infrared spectroscopy (Figure S2a) and in-air thermogravimetry (Figure S2b) analyses allowed us determining the general chemical formula as $Ni(OH)_{1-x}(CH_3CO_2)_x.nH_2O$ x ≈ 0.4 and n ≈ 0.6, close to that of nickel hydroxyacetate salts described in previous works [1]. Indeed, the recorded FTIR spectrum evidenced two large bands at 1611 and 1382 cm^{-1}, due to COO stretching and a third band at 1423 cm^{-1} due to CH_3 deformation, which can be the fingerprint of acetate species. Hydroxyl groups and water signature were also evidenced by the broad bands observed at high frequency, at 3398 and 3549 cm^{-1} [1,2]. Alkyle C-H stretching bands were also identified at 2923 and 2858 cm^{-1}, originated from structural acetate, as well as CH_3 rocking and deformation band at 1100-1000 cm^{-1} [3]. Besides the weight loss and the heat flow variation as a function of temperature inferred from the thermogravimetry analysis were plotted evidencing the hydroxide derivative decomposition into NiO (confirmed by the XRD analysis of the heated residue). Several mass losses were observed: First an endothermic departure of adsorbed water at 60°C, second several exothermic weight losses between 240-285 °C involving H_2O and CO_2 formation through the hydroxide dehydratation and acetate combustion.

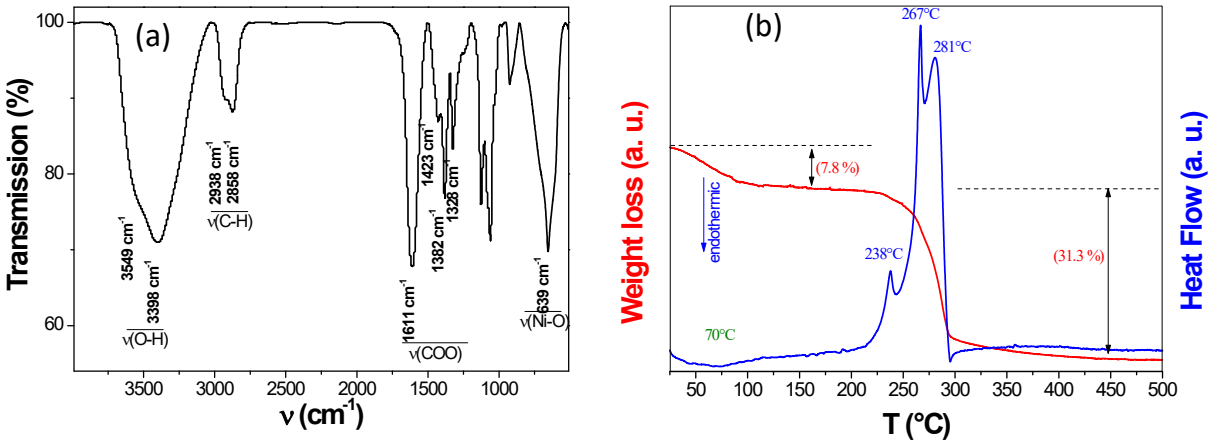

Figure S2. a) FTIR spectrum of the as-produced nickel hydroxyacetate derivative powder and b) its thermogravimetry plots recorded in air for a heating at 10°C.min^{-1} up to 500°C.

[1] Poul L, Jouini N, Fievet F. Layered Hydroxide Metal Acetates (Metal = Zinc, Cobalt, and Nickel): Elaboration via Hydrolysis in Polyol Medium and Comparative Study, *Chem. Mater.*, 2000, **12**, 3123-32 https://doi.org/10.1021/cm991179j

[2] Kooli F, Chisem IC, Vucelic M, Jones W. Synthesis and Properties of Terephthalate and Benzoate Intercalates of Mg–Al Layered Double Hydroxides Possessing Varying Layer Charge, *Chem. Mater.*, 1996, **8**, 1969-77. https://doi.org/10.1021/cm960070y

[3] L. H. Jones, M. MacLaren, Infrared spectra of CH_3COONa and CD_3COONa and assignements of vibrational frequencies, *J. Chem. Phys.*, 1954, **22**, 1796-1800. https://doi.org/10.1063/1.1739921

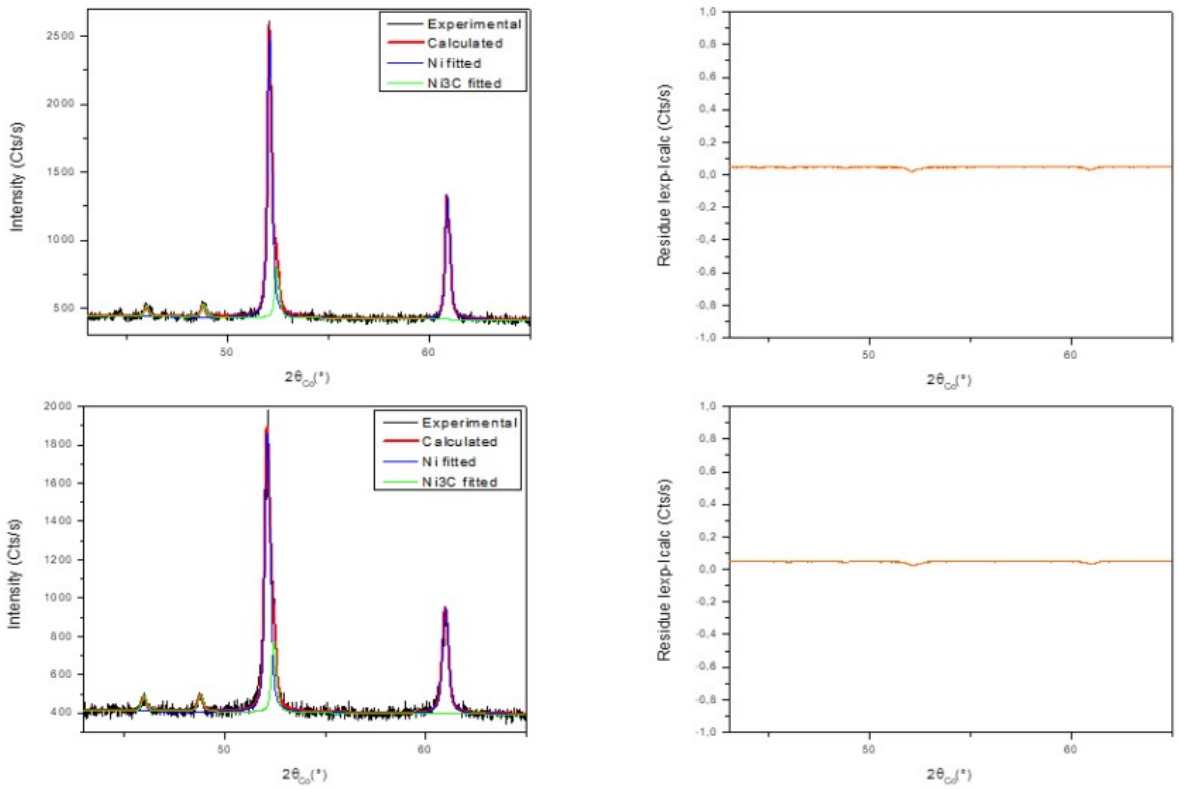

Figure S3. Experimental (black line) and calculated (red line) XRD patterns of the 6 (upper graphs) and 8 h (lower graphs) plasma treated nickel hydroxyacetate derivative. The residue, defined as the difference between the experimental and calculated diffractograms, is given (orange line) to illustrate the fit quality. Note, a pseudo-Voigt function was used for modelling the peak profile. A set of about 15 parameters was then refined, including the scale factor, the zero shift, the background polynomial coefficients, the peak profile parameters, and for each constituting phase, the cell parameter, the average crystallographic coherence length, assuming isotropic crystals, the average lattice micro-deformation and the weight ratio. As a first approximation, the atomic coordinates of all the atoms, and their isotropic temperature factors were fixed. In all the cases, the fitting was achieved with reliability Bragg factor R_B values close to 2.

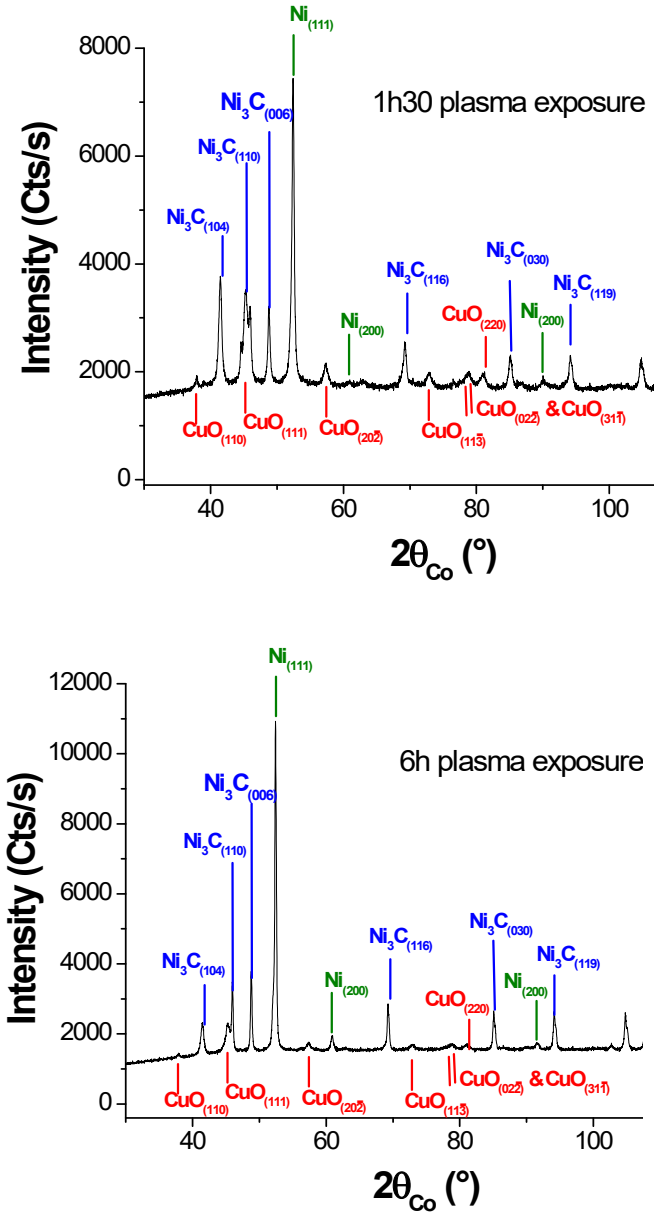

Figure S4. XRD patterns of two representative sample series recorded after mixing the produced powders with with a powdered strain free large grain CuO reference to exclude any sample diffraction misalignment and/or goniometer zero offset effect on the collected data.

Table S1. calculated reticular d_{hlk} distances for both cubic NiC_x and rhombohedric Ni_3C phases using the inferred unit cell parameters *a* and *c*, from Rietveld refinements using the well-known relations between d_{hlk} , *a, c* and the Miller indexes in both cubic and hexagonal phases.

$$d_{hkl} = \frac{a}{\sqrt{h^2 + k^2 + l^2}} \qquad d_{hkl} = \frac{1}{\sqrt{\frac{4}{3\,a^2}(h^2 + k^2 + hk) + \frac{l^2}{c^2}}}$$

plasma exposure time /h	h	k	l	$d_{hkl}(NiC_x)$ / Å	d_{hkl} (Ni_3C) / Å
2	2	0	0	1.7685	-
	1	0	-2	-	3.3878
	-1	2	0	-	2.2915
	0	0	6	-	2.1675
6	1	1	0	-	2.2910

	2	-1	0	-	2.2910
	2	0	2	-	1.8978
	1	1	1	2.0386	-

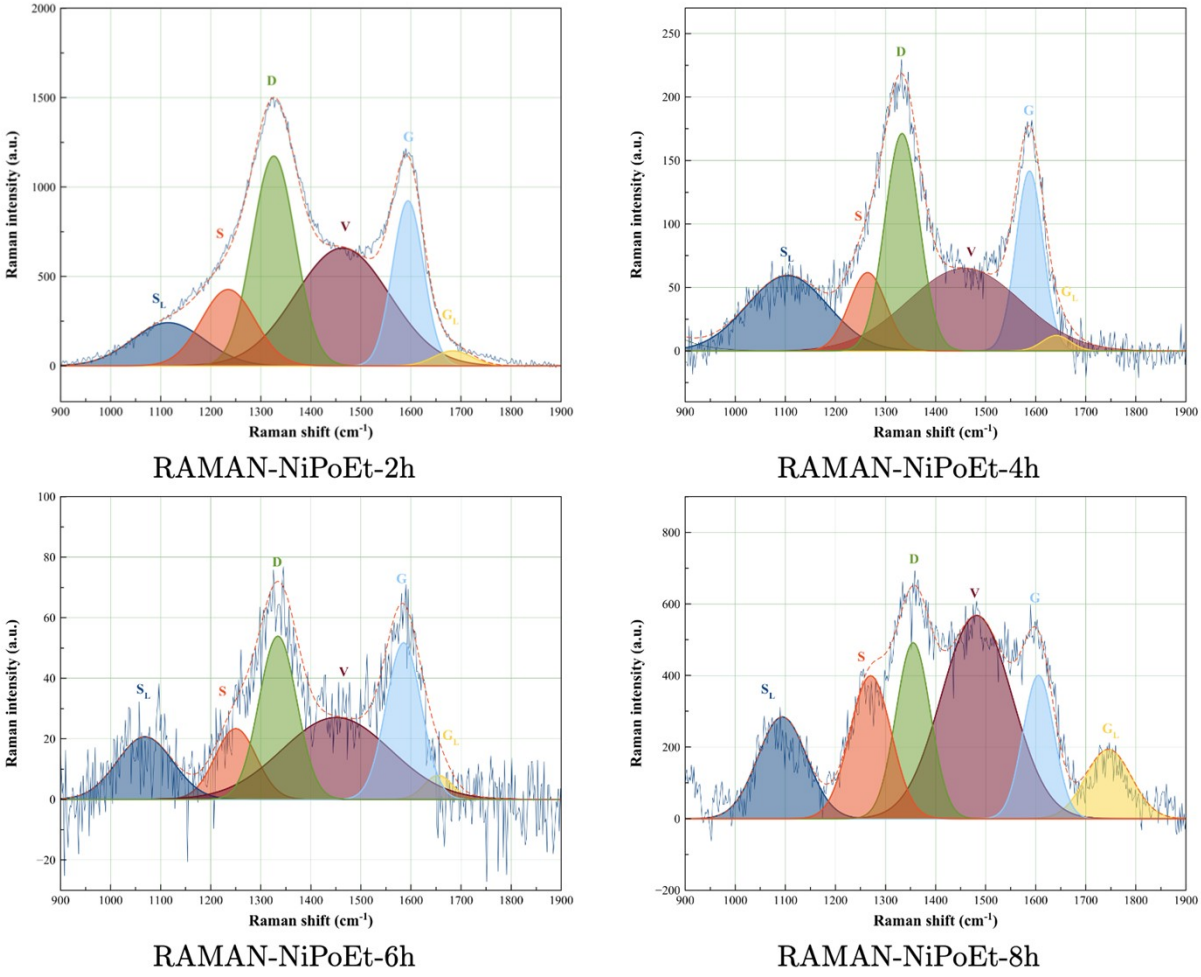

Figure S5. Deconvolution of the Raman spectra recorded on the 90-10% H_2-Ar plasma treated nickel hydroxide derivative for different exposure times (2, 4, 6 and 8 h).

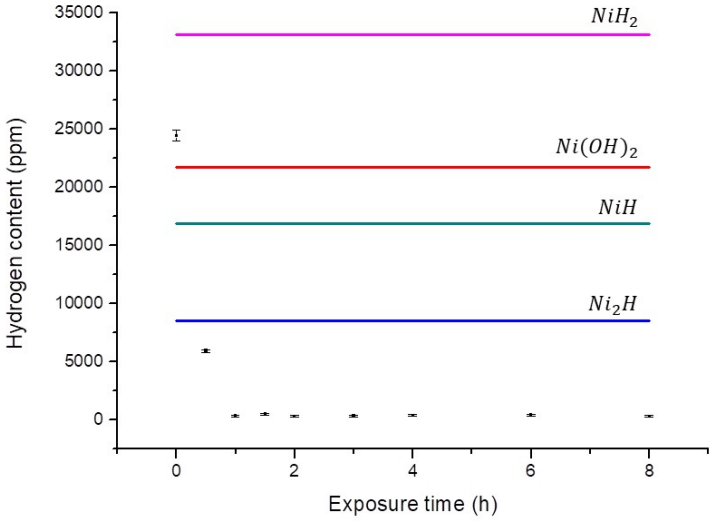

Figure S6. Results of hydrogen quantification experiments on the freshly plasma treated nickel hydroxyacetate derivative for different exposure times. The horizontal colored lines correspond to the expected hydrogen content in bulk NiH, Ni_2H, NiH_2 and $Ni(OH)_2$ as reference compounds. The obtained plot, clearly showed that pure hydroxide precursor is consistent with the largest hydrogen release, slightly higher than that expected for $Ni(OH)_2$ phase, in agreement with its hydrogen richer content (structural hydroxyl, water and acetate groups and adsorbed polyol residues). But rapidly, as the hydroxide derivative disappeared as the amount of released hydrogen decreased drastically down to 300 ppm after only one hour of plasma treatment and 0 ppm after two hours.

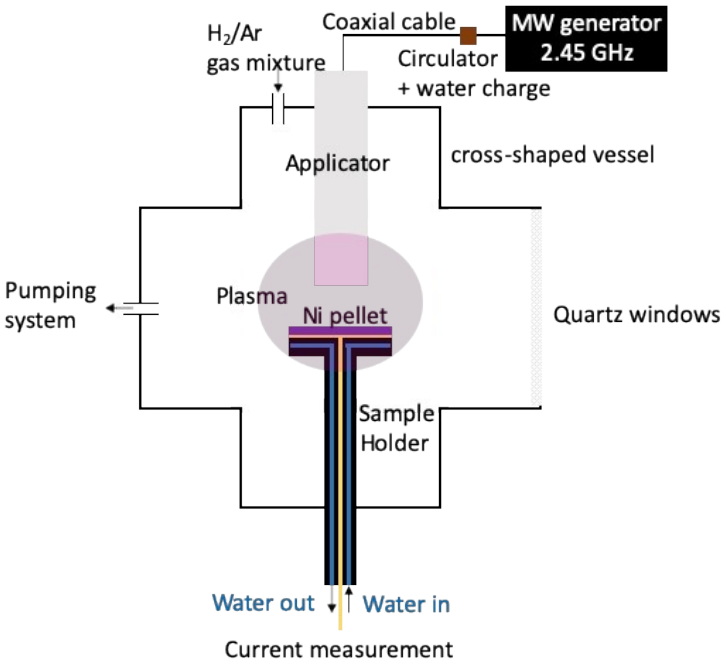

Figure S7. Scheme of the plasma reactor. It consists of a cross-shaped stainless steel vessel with a total volume of 5 dm^3. It has 6 ports or openings (DN 100) which have multiple uses: pumping system, sample holder, plasma source and plasma diagnostics through quartz windows. The system is composed of two pumps: a primary dry pump (Alcatel ACPA15) and a turbo-molecular pump (Pfeiffer) with a pumping rate of 250 $L.s^{-1}$ that allows reaching a vacuum limit of 10^{-6} mbar. The pressure is measured by an MKS capacitive gauge (range 1 mbar). The reactor has a manual valve in front of the pumping system that allows isolating the reactor when needed. The gas flow is controlled by Bronkhorst flowmeters. Each flowmeter is calibrated for the gas it controls (from 0 to 100 sccm).